

Electronic Supplementary Information

Optimizing Surface State of Cobalt-Iron Bimetallic Phosphide via Regulating Phosphorus Vacancies

Shuang Li,^{‡a} Zhibin Geng,^{‡a} Xiyang Wang,^a Xiaoru Ren,^a Jinghai Liu,^b Xiangyan Hou,^a Yu Sun,^a Wei Zhang,^c Keke Huang^{*a} and Shouhua Feng^a

Experimental Section

Synthesis of the CoFe LDHs: The CoFe LDHs were synthesized by a typical hydrothermal method.¹ First, 0.3 M Fe(NO₃)₃·9H₂O and 0.6 M Co(NO₃)₂·6H₂O were dissolved in deionized water in a beaker and 1.92 M NaOH and 0.8 M Na₂CO₃ were dissolved in deionized water in another beaker. Second, equal volumes of two solutions were mixed and added simultaneously to a beaker under vigorous stirring. Third, the mixed solution (60 ml) was transferred to a stainless-steel Teflon-lined autoclave (100 ml), which was then reacted in a preheated oven at 80 °C for 48 h. Finally, the obtained precursor was washed with water three times and then it was freeze-dried.

Synthesis of the Co_{0.68}Fe_{0.32}P: The lyophilized CoFe LDHs (20 mg) and 1.5 g NaH₂PO₂ were placed at two separate quartz boats with NaH₂PO₂ at the upstream side of the tube furnace. Subsequently, the samples were heated at 300 °C for 3 h under a flowing Ar atmosphere with a heating rate of 5 °C min⁻¹. Then the samples were naturally cooled down to room temperature in Ar flow.

Synthesis of the Ar-plasma etched Co_{0.68}Fe_{0.32}P: 20 mg Co_{0.68}Fe_{0.32}P was spread on the watch glass in a plasma reactor. Next, the samples were treated by Ar-plasma with a power of 300 W and pressure of 50 Pa and the treatment time is 30 min, 60 min, 90 min, respectively.

Electrochemical Characterization: The as-prepared catalysts (5 mg), Vulcan carbon black (VB, 1 mg) were dissolved in 1 mL of a mixed water-isopropanol (1:1 v/v) solution, and then 30 μL of 5 wt% Nafion solution was added as the binder. After sonication for 30 min, 8 μL of the suspension was loaded onto the surface of a glassy carbon electrode (3 mm in diameter) and air-dried naturally at room temperature.² The electrochemical measurements were carried out using a CHI 660E electrochemical workstation (CH Instruments, Inc., Shanghai) in a standard three-electrode setup. A mercuric oxide electrode was used as a reference electrode and a graphite electrode as a counter

electrode. The electrocatalytic activities of the samples toward OER were examined by obtaining polarization curves using LSV with a scan rate of 5 mV s^{-1} at room temperature in 1 M KOH solution using a typical three-electrode setup with the loading of 0.33 mg cm^{-2} on a glassy carbon electrode. The stability tests of the $\text{Co}_{0.68}\text{Fe}_{0.32}\text{P-60}$ was performed by potential cycling from 0.1 to 0.2 V (vs RHE) at a sweep rate of 100 mV s^{-1} in 1 M KOH for 1000 cycles, then linear sweep voltammetry polarization curves were obtained. All the polarization curves were corrected by eliminating iR drop with respect to the ohmic resistance of the solution. All the potentials reported in this work were converted to the RHE.

Catalyst Characterization: Powder X-ray diffraction (XRD) patterns were recorded with a D/Max 2500 V/PC X-ray diffractometer from Rigaku company with $\text{CuK}\alpha$ radiation ($\lambda = 1.5418 \text{ \AA}$) at 50 kV and 200 mA, the scanning speed was set at 1° min^{-1} at room temperature. Scanning electron microscope (SEM) images were recorded by a Helios NanoLab 600i Dual Beam System from FEI Company. High-resolution transmission electron microscopy (HRTEM) images were determined with a Tecnai F20 electron microscope from FEI Company operated at 200 kV. Inductively Coupled Plasma-Atomic Emission Spectrometry (ICP-AES) was used to determine the chemical composition of the samples. X-ray photoelectron spectra (XPS) were recorded with an ESCALAB 250Xi electron energy spectrometer from Thermo company using $\text{Al K}\alpha$ (1486.6 eV) as the X-ray excitation source. X-ray absorption near-edge spectra (XANES) of the Co *L*-edge, Fe *L*-edge and P *L*-edge were measured at the BL12B-a beamline of the National Synchrotron Radiation Laboratory (NSRL) in China. Electron paramagnetic resonance (EPR) spectra was recorded by Bruker E500.

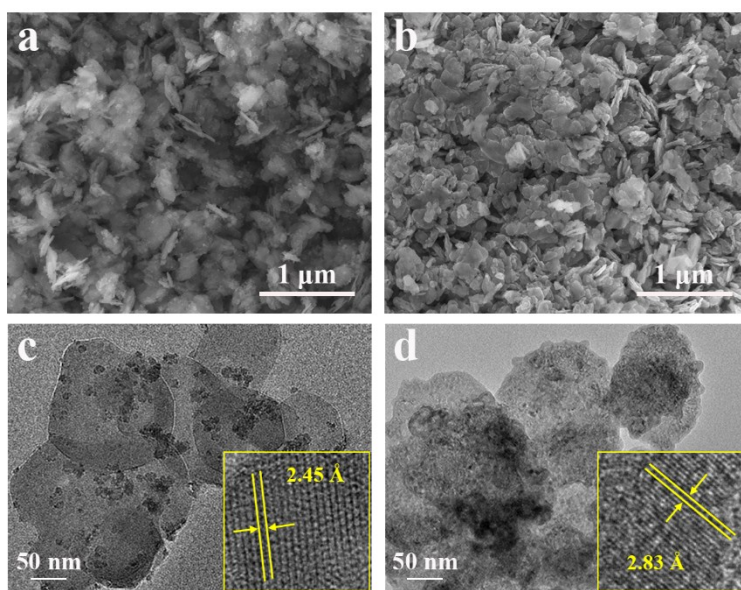


Figure S1. SEM images of (a) CoFe LDHs and (b) $\text{Co}_{0.68}\text{Fe}_{0.32}\text{P}$. TEM images of (c) and CoFe LDHs (d) $\text{Co}_{0.68}\text{Fe}_{0.32}\text{P}$, and the corresponding insets show HRTEM images.

In Figure S1a and S1c, the diameter of CoFe LDHs nanosheets is 100-200 nm. In Figure S1b and S1d, the surface of the nanosheets becomes rough after phosphating, and $\text{Co}_{0.68}\text{Fe}_{0.32}\text{P}$ might be a little agglomerated after annealing. The lattice fringes are given in Figure S1c and 1d belong to (104) facets of CoFe LDHs and (011) facets of $\text{Co}_{0.68}\text{Fe}_{0.32}\text{P}$, respectively, the corresponding lattice spacing is 2.45 Å and 2.83 Å.

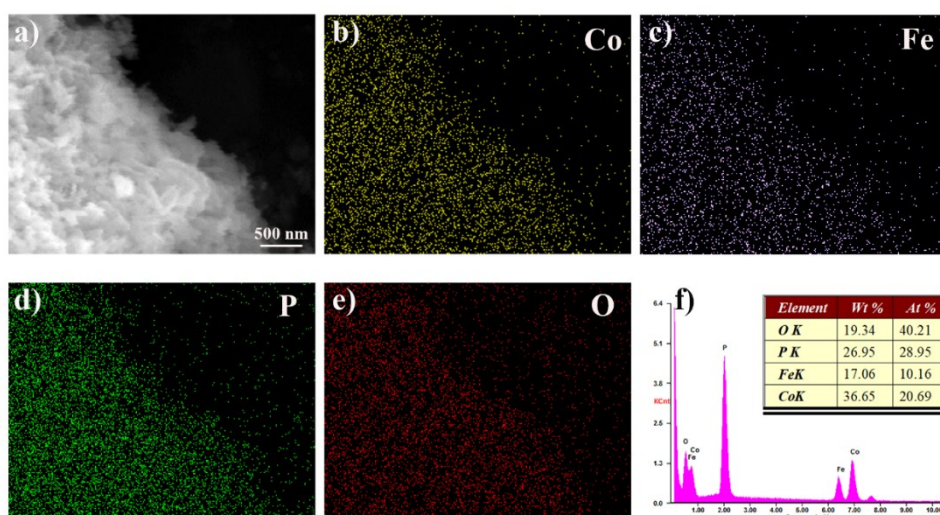


Figure S2. SEM image (a) and the typical EDX elemental mapping of $\text{Co}_{0.68}\text{Fe}_{0.32}\text{P}$: (b) Co, (c) Fe, (d) P and (e) O. (f) EDX spectrum. The values are just for references.

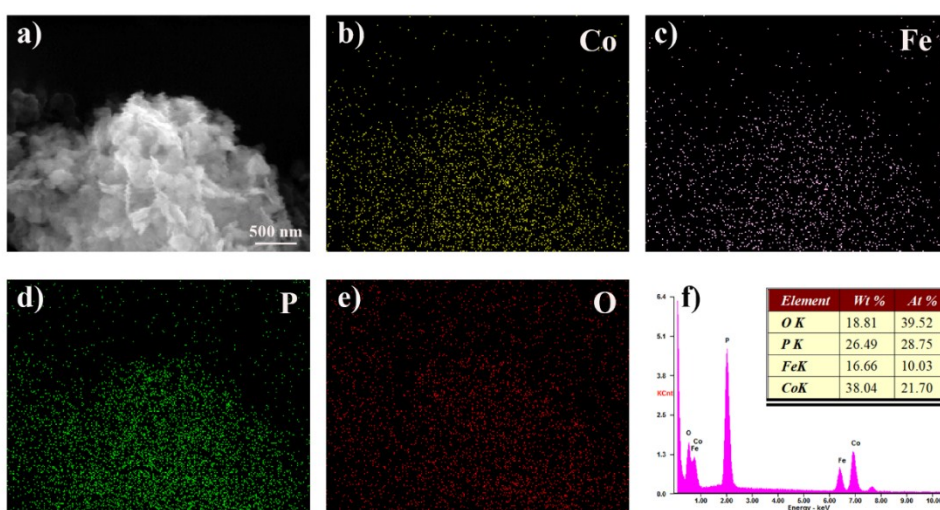


Figure S3. SEM image (a) and the typical EDX elemental mapping of $\text{Co}_{0.68}\text{Fe}_{0.32}\text{P-60}$: (b) Co, (c) Fe, (d) P and (e) O. (f) EDX spectrum. The values are just for references.

Figure S2 and S3 show the selected area energy dispersive X-ray spectrum (EDX) elemental mapping and the corresponding EDX for $\text{Co}_{0.68}\text{Fe}_{0.32}\text{P}$ and $\text{Co}_{0.68}\text{Fe}_{0.32}\text{P-60}$. That further confirms the existence of Co, Fe, O, and P elements, which reveals a uniform distribution of Co, Fe, and P in the samples. Besides, the EDX spectrum indicates the presence of Co and Fe with an atomic ratio is approximately 0.68/0.32, which is consistent with the ICP results.

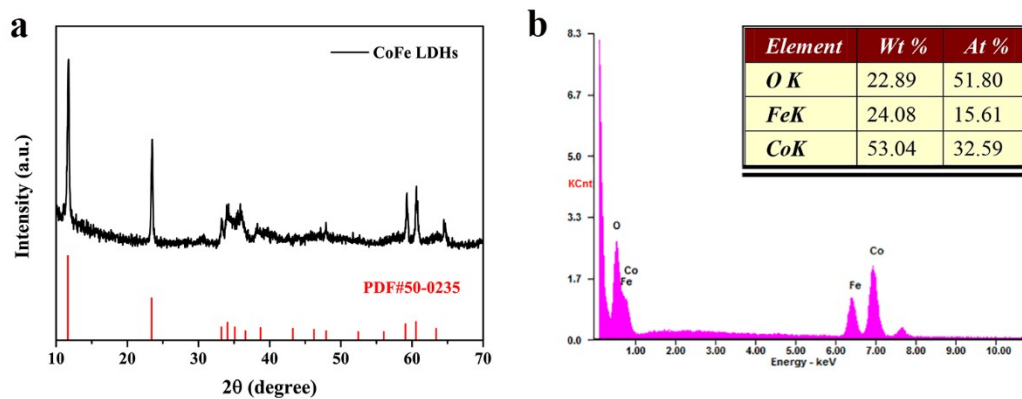


Figure S4. (a) XRD pattern of the CoFe LDHs compared to the standard X-Ray diffraction pattern of hexagonal (PDF # 50-0235). (b) EDX spectrum of CoFe LDHs. The values are just for references.

The XRD patterns of CoFe LDHs (Figure S4a) show sharp peaks at 11.6° and 23.4° , individually corresponding to (003) and (006) planes of CoFe LDHs nanosheets (JCPDF No. 50-0235).^{3,4}

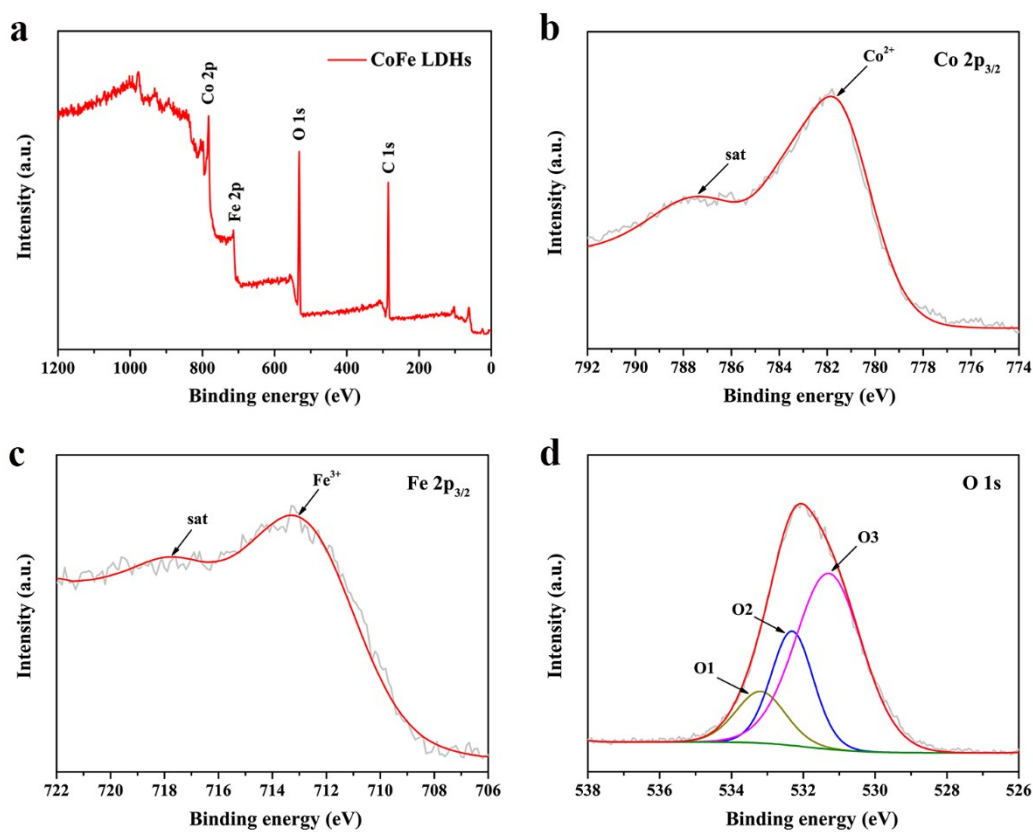


Figure S5. XPS spectra of CoFe LDHs: (a) survey scans, (b) Co 2p_{3/2}, (c) Fe 2p_{3/2} and (d) O 1s.

For CoFe LDHs, as shown in Figure S5, the Co 2p spectrum of the Co 2p_{3/2} exhibits a peak at 781.5 eV which can be attributed to Co²⁺-OH bonds; the Fe 2p spectrum of the Fe 2p_{3/2} exhibits a peak at 712.7 eV which can be attributed to Fe³⁺-OH bonds; the O 1s spectrum is composed of three peaks and the binding energy at 533.2eV (O1) is based on the adventitious carbon oxygen species and surface adsorbed molecular water, binding energy at 532.3 eV (O2) corresponds to surface-adsorbed oxygen, binding energy at 531.3 eV (O3) can be associated with defects with a low oxygen coordination.^{1,5}

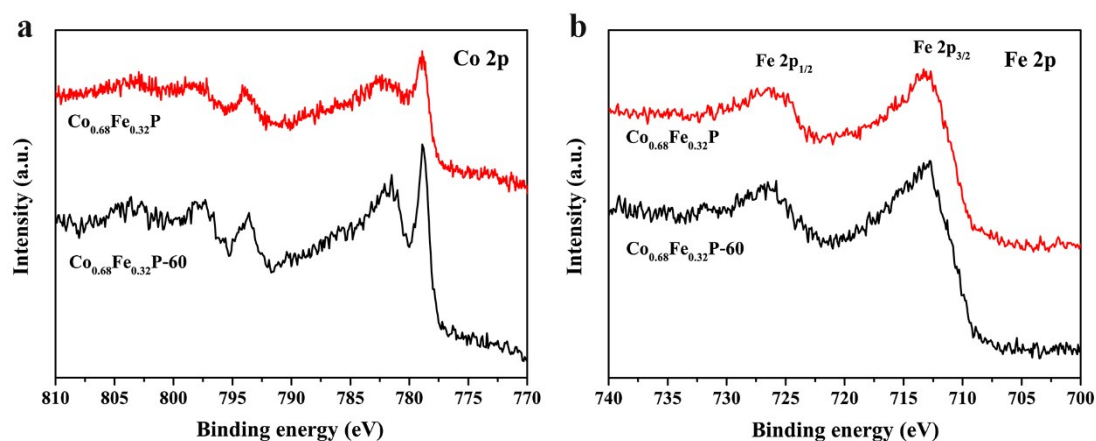


Figure S6. XPS spectra of $\text{Co}_{0.68}\text{Fe}_{0.32}\text{P-60}$ and $\text{Co}_{0.68}\text{Fe}_{0.32}\text{P}$: (a) Co 2p and (b) Fe 2p.

Co 2p and Fe 2p spectrum are shown in Figure S6, and the peaks at 778.8 and 129.6 eV are close to the binding energies of Co and P in CoP, and the peak at ~ 782 eV was assigned to the oxidized cobalt species.⁶⁻⁹ Figure S6b shows that Fe 2p spectrum has two main peaks at 713.2 and 726.6 eV, corresponding to Fe 2p_{3/2} of iron oxides, and Fe 2p_{1/2}. $\text{Co}_{0.68}\text{Fe}_{0.32}\text{P-60}$ and $\text{Co}_{0.68}\text{Fe}_{0.32}\text{P}$ have almost the same peak position of X-ray photoelectron spectroscopy as Co 2p and Fe 2p.

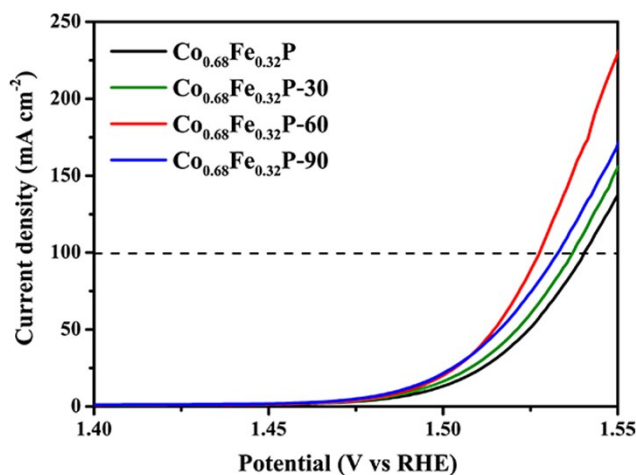


Figure S7. The OER performances of $\text{Co}_{0.68}\text{Fe}_{0.32}\text{P}$ by Ar-plasma treatment for different time.

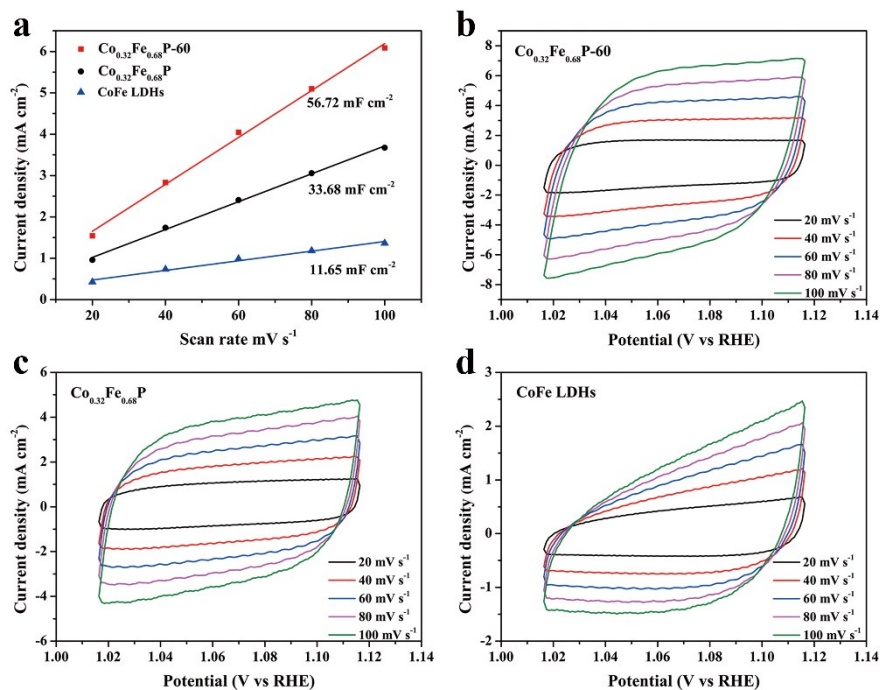


Figure S8. (a) Current density variation plotted against scan rate fitted to a linear regression for the estimation of the double layer capacitance (C_{dl}). Cyclic voltammograms at different scan rates of (b) $\text{Co}_{0.68}\text{Fe}_{0.32}\text{P-60}$, (c) $\text{Co}_{0.68}\text{Fe}_{0.32}\text{P}$ and (d) CoFe LDHs to estimate of electrochemical active surface area (ECSA).

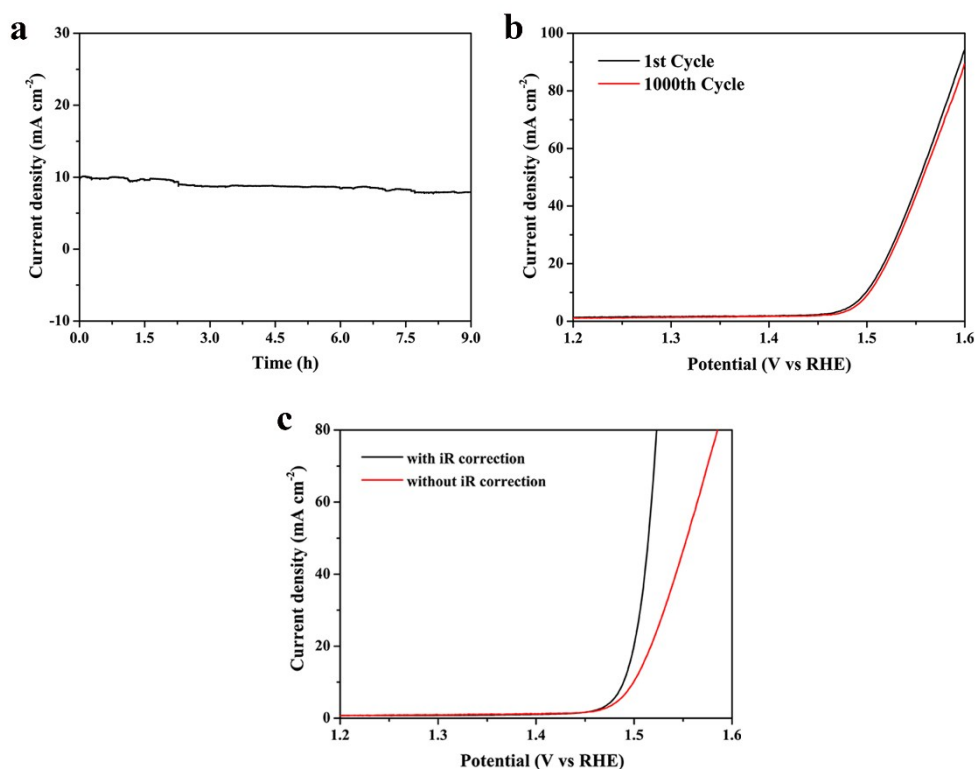


Figure S9. (a) Time dependent current density of Co_{0.68}Fe_{0.32}P-60. OER Polarization curves of Co_{0.68}Fe_{0.32}P-60 (b) before and after 1000 potential cycles and (c) with and without iR correction.

In order to verify the stability of the Co_{0.68}Fe_{0.32}P-60, we adopted continuous cyclic voltammetry (CV) in the range of 1.0~1.1 V versus RHE at a scan rate of 10 mV s⁻¹ at room temperature. In Figure S9a, there is almost no much difference between the original LSV polarization curve and one after 1000 cycles, confirming that Co_{0.68}Fe_{0.32}P-60 has excellent stability during the continuous CV tests.

Table S1. Summary of the electrochemical water oxidation activities of Co-based metal phosphides.

Catalyst	Electrolyte	η at 10 mA cm ⁻² (mV)	Ref.
Co_{0.68}Fe_{0.32}P-60	1M KOH	259	This work
R-CoPx/rGO(O)	1M KOH	268	10
Co_{0.7}Fe_{0.3}P/CNTs	1M KOH	243	11
Co_{0.68}Fe_{0.32}P	1M KOH	289	12
Co-P/NC	1M KOH	354	13
CoP₃ NAs/CFP	1M KOH	334	14
Co/CoP-5	1M KOH	340	15
CoP-based nano Needle	1M KOH	281	16
CoP₂/RGO	1M KOH	300	17
CoP hollow polyhedron	1M KOH	400	18
CoMnP	1M KOH	330	19

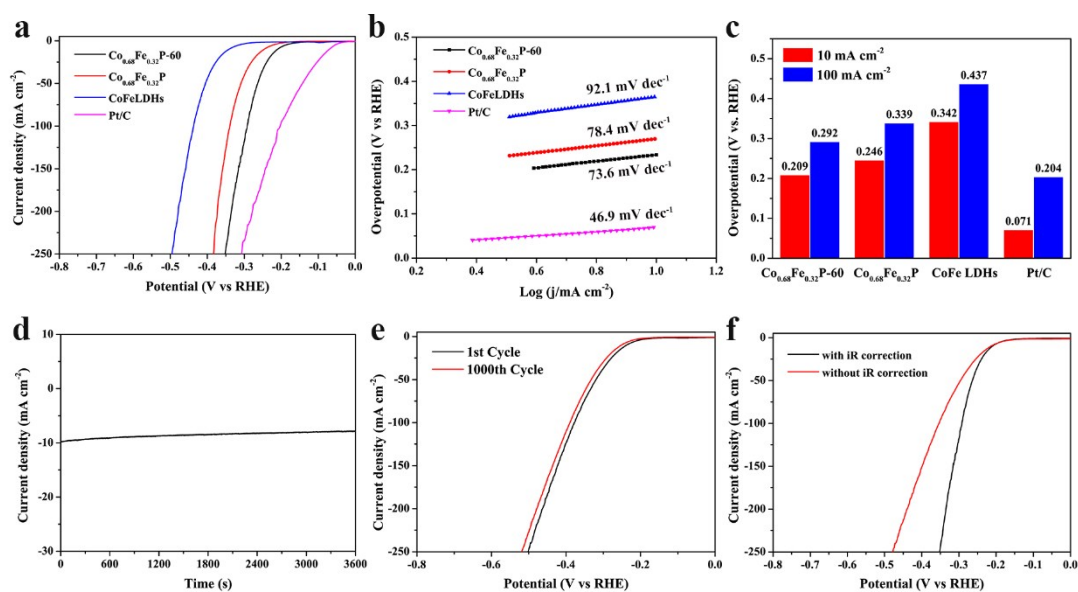


Figure S10. HER analyses of $\text{Co}_{0.68}\text{Fe}_{0.32}\text{P-60}$, $\text{Co}_{0.68}\text{Fe}_{0.32}\text{P}$, CoFe LDHs and Pt/C electrocatalysts in 1.0 M aq. KOH solution: (a) Polarization curves. (b) Tafel plots. (c) Overpotentials at the rate 10 mA cm^{-2} and 100 mA cm^{-2} . (d) Time dependent current density of $\text{Co}_{0.68}\text{Fe}_{0.32}\text{P-60}$. (e) Polarization curves of $\text{Co}_{0.68}\text{Fe}_{0.32}\text{P-60}$ before and after 1000 potential cycles. (f) Polarization curves of $\text{Co}_{0.68}\text{Fe}_{0.32}\text{P-60}$ with and without iR correction.

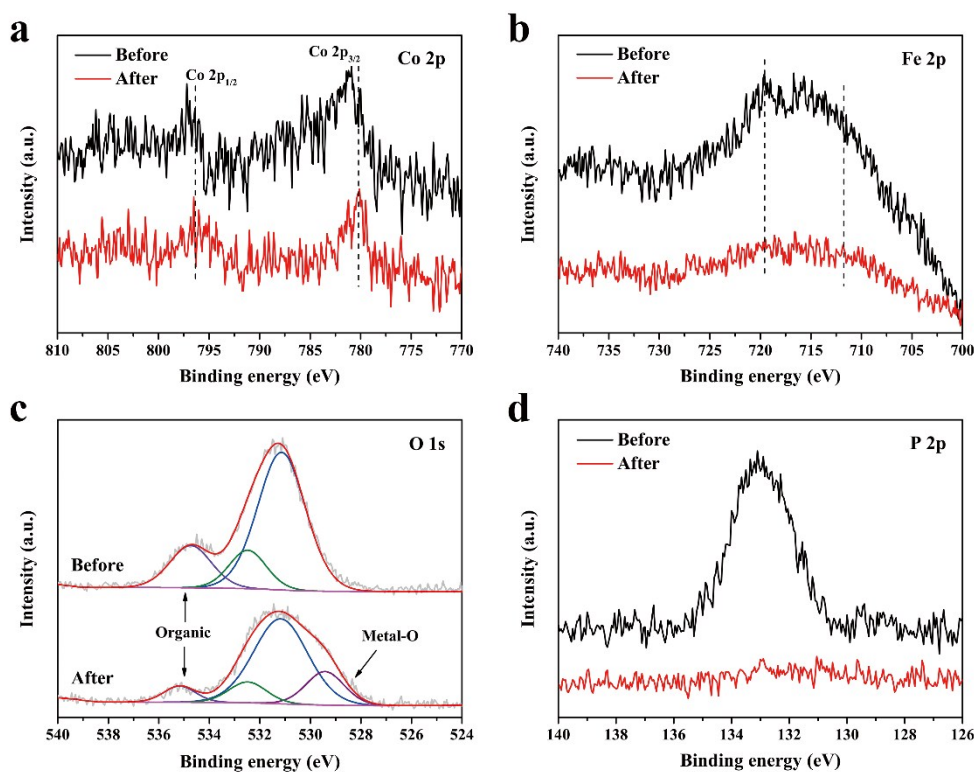


Figure S11. XPS spectra of $\text{Co}_{0.68}\text{Fe}_{0.32}\text{P-60}$ before and after electrolysis: (a) Co 2p, (b) Fe 2p, (c) O 1s and (d) P 2p.

In an effort to understand the OER mechanism, we performed XPS analysis on the $\text{Co}_{0.68}\text{Fe}_{0.32}\text{P-60}$ (as prepared suspension) dropped on carbon paper before and after the electrochemical reaction. In Figure S11d, the P 2p signal disappears after catalytic cycling, suggesting that the P element at the surface of $\text{Co}_{0.68}\text{Fe}_{0.32}\text{P-60}$ is etched.^{6,19} The Co 2p_{3/2} spectrum exhibits a primary peak centered at 780.2 eV (Figure S11a), which can be ascribed to the binding energy for Co in CoOOH.¹¹ Besides, Fe 2p_{3/2} spectrum exhibits a primary peak centered at 711.8 eV (Figure S11b), which can be ascribed to the binding energy for Fe in FeOOH.^{11,20} These results indicate that the surface of $\text{Co}_{0.68}\text{Fe}_{0.32}\text{P-60}$ is mostly transformed into oxy-hydroxide, which is the active species for OER after electrochemical oxidation under the OER conditions.^{11,20-22}

References

- (1) Y. Y. Wang, C. Xie, Z. Y. Zhang, D. D. Liu, R. Chen and S.Y. Wang, *Adv. Funct. Mater.*, 2018, **28**, 1703363.
- (2) F. B. Shi, Z. B. Geng, K. K. Huang, Q. S. Liang, Y. Zhang, Y. Sun, J. G. Cao and S. H. Feng, *Adv. Sci.*, 2018, **5**, 1800575.
- (3) V. Rives, *Mater. Chem. Phys.*, 2002, **75**, 19-25.
- (4) R. Liu, Y. Y. Wang, D. D. Liu, Y. Q. Zou and S. Y. Wang, *Adv. Mater.* 2017, **29**, 1701546.
- (5) L. Z. Zhuang, L. Ge, Y. S. Yang, M. R. Li, Y. Jia, X. D. Yao and Z. H. Zhu, *Adv. Mater.*, 2017, **29**, 1606793.
- (6) M. Jiang, J. Li, X. F. Cai, Y. Zhao, L. J. Pan, Q. Q. Cao, D. H. Wang and Y. W. Du, *Nanoscale*, 2018, **10**, 19774-19780.
- (7) Q. Liu, J. Q. Tian, W. Cui, P. Jiang, N. Y. Cheng, A. M. Asiri and X. P. Sun, *Angew. Chem. Int. Ed.*, 2014, **53**, 6710-6714.
- (8) Y. X. Lin, L. Yang, Y. K. Zhang, H. L. Jiang, Z. J. Xiao, C. Q. Wu, G. B. Zhang, J. Jiang and L. Song, *Adv. Energy Mater.*, 2018, **8**, 1703623.
- (9) P. Jiang, Q. Liu, C. Ge, W. Cui, Z. Pu, A. M. Asiri and X. Sun, *J. Mater. Chem. A.*, 2014, **2**, 14634.
- (10) X. C. Zhou, H. Gao, Y. F. Wang, Z. Liu, J. Q. Lin and Y. Ding, *J. Mater. Chem. A.*, 2018, **6**, 14939-14948.
- (11) X. Zhang, X. Zhang, H. M. Xu, Z. S. Wu, H. L. Wang and Y. Y. Liang, *Adv. Funct. Mater.*, 2017, **27**, 1606635.
- (12) F. Li, Y. F. Bu, Z. J. Lv, J. Mahmood, G. F. Han, I. Ahmad, G. Kim, Q. Zhong and J. B. Baek, *Small*, 2017, **13**, 1701167.

- (13) B. You, N. Jiang, M. L. Sheng, S. Gul, J. Yano and Y. J. Sun, *Chem. Mater.*, 2015, **27**, 7636-7642.
- (14) T. L. Wu, M. Y. Pi, D. K. Zhang and S. J. Chen, *J. Mater. Chem. A.*, 2016, **4**, 14539-14544.
- (15) Z. H. Xue, H. Su, Q. Y. Yu, B. Zhang, H. H. Wang, X. H. Li and J. S. Chen, *Adv. Energy Mater.*, 2017, **7**, 1602355.
- (16) P. Wang, F. Song, R. Amal, Y. H. Ng and X. L. Hu, *ChemSusChem.*, 2016, **9**, 472-477.
- (17) J. M. Wang, W. R. Yang and J. Q. Liu, *J. Mater. Chem. A.*, 2016, **4**, 4686-4690.
- (18) M. J. Liu and J. H. Li, *ACS Appl. Mater. Inter.*, 2016, **8**, 2158-2165.
- (19) D. Li, H. Baydoun, C. N. Verani and S. L. Brock, *J. Am. Chem. Soc.*, 2016, **138**, 4006-4009.
- (20) D. Friebe, M. W. Louie, M. Bajdich, K. E. Sanwald, Y. Cai, A. M. Wise, M. J. Cheng, D. Sokaras, T. C. Weng, R. A. Mori, R. C. Davis, J. R. Bargar, J. K. Norskov, A. Nilsson and A. T. Bell, *J. Am. Chem. Soc.*, 2015, **137**, 1305-1313.
- (21) A. Dutta and N. Pradhan, *J. Phys. Chem. Lett.*, 2017, **8**, 144-152.
- (22) M. S. Burke, M. G. Kast, L. Trotochaud, A. M. Smith and S. W. Boettcher, *J. Am. Chem. Soc.*, 2015, **137**, 3638-3648.